

On Spacetime Quantum Duality and Bounce Cosmology of a Dual Universe

Mohammed. B. Al-Fadhli^{1*}

¹College of Science, University of Lincoln, Lincoln, LN6 7TS, UK.

*Correspondence: malfadhli@lincoln.ac.uk; mo.fadhli7@gmail.com

Abstract: The recent Planck Legacy release confirmed the existence of an enhanced lensing amplitude in the cosmic microwave background (CMB) power spectra, which endorses the positive curvature of the early Universe with a confidence level exceeding 99%. In this study, the pre-existing curvature is incorporated to extend the field equations where the derived wave function of the Universe is utilized to model Universe evolution with reference to the scale factor of the early Universe and its radius of curvature upon the emission of the CMB. The wave function reveals both positive and negative solutions, implying that matter and antimatter of early Universe plasma evolve in opposite directions as distinct Universe sides. The wave function indicates that a nascent hyperbolic expansion is followed by a first phase of decelerating expansion away from early plasma during the first ~ 10 Gyr, and then, a second phase of accelerating expansion in reverse directions, whereby both Universe sides free-fall towards each other under gravitational acceleration. Simulations of the predicted conformal curvature evolution demonstrate the fast orbital speed of outer stars owing to the external fields exerted on galaxies as they travel through conformally curved space-time. Finally, the wave function predicts an eventual time-reversal phase comprising rapid spatial contraction that culminates in a Big Crunch, signalling a cyclic Universe. These findings reveal that early plasma could have separated and evolved into distinct sides that collectively and geometrically influencing the Universe evolution, physically explaining the effects attributed to dark matter and energy.

Keywords: Accelerated Expansion; Fast orbital speed of outer stars; Duality; Antimatter.

1. INTRODUCTION

Bounce cosmology provides an alternative view of the Universe, in which our Universe expanded from a hot and very dense state of a previous collapsed Universe [1]. This cosmology is free from the singularity problem and offers a clearer view of the early Universe. However, the null-energy condition is generally violated by the conjectured bounce of re-expansion in several modified gravity theories [2]. Alternatively, this bounce could be realized through other scenarios, such as the phenomenon of plasma drift in the presence of electromagnetic fields. In this sense, matter and antimatter in early Universe plasma could be separated by primordial electromagnetic fields upon the emission of the cosmic microwave background (CMB), thereby evolving in opposite directions owing to their opposite spin and charge. The plasma separation until and under the right conditions would allow the collapsed state to achieve thermal equilibrium while the gravitational contributions of early Universe plasma boundary could realize a singularity-free paradigm. Signs of the plasma separation or a significant predominant event might be observed as associated noise surrounding the measured gravitational waves [3]. Additionally, the magnetic fields that presently pervade the Universe at all probed scales favour a primordial origin of this kind [4].

The Planck Legacy PL18 release confirmed the existence of an enhanced lensing amplitude in the power spectra of the CMB [5]. Notably, it is more than that estimated by the Λ CDM model (Λ CDM), which endorses the positive curvature of the early Universe with a confidence level more than 99% [5,6]. Besides, the observed gravitational lensing by substructures of several galaxy clusters is an order of magnitude higher than that estimated by the Λ CDM [7,8]. This endorses a curved Universe despite of the present/local space-time flatness.

The presumed concepts of dark energy, dark matter, and antimatter early elimination are being challenged by new observations and measurements. Riess in 2020 found the Universe expansion is faster than the Λ CDM estimates [9] while Ryskin showed that vacuum energy cannot be causing the accelerated expansion [10]. In addition, external field effect that influence galactic rotation curves were detected at up to 8σ to 11σ , challenging traditional dark matter concepts [11]. Additionally, advanced measurements of the fine structure of hydrogen and antihydrogen atoms were found to be consistent with Quantum Electrodynamics Theory predictions at a margin of 2%, including the Lamb-shift feature, undermining elimination assumptions [12].

Accordingly, a closed early Universe model is considered in this study to approach the problems of accelerated expansion and fast orbital speed of stars from a new perspective. The closed finite Universe can provide an agreement with the CMB anisotropy observations [13] and could explain the quantum entanglement, where the total Universe energy is finite; thus, cosmic conservation preserves the total spin of a pair of particles regardless of their locations [14]. The pre-existing curvature is considered to extend the field equations and the evolution of the Universe from early plasma is modelled by utilising the Universe wave function. This paper is organised as follows. Section 2 presents the extended field equations. Sections 3 and 4 discuss the Universe model, its evolution, and its minimal radius while Section 5 presents the spiral galaxy simulation under external fields. Finally, section 6 concludes this work and suggests future works.

2. Extended Field Equations for the Curved Early Universe

The recent PL18 release revealed a positive early Universe curvature, that is, is evidence of a pre-existing or background curvature. To consider this pre-existing curvature and its evolution over cosmic time, t , a modulus of spacetime deformation, E_D , is utilized. Spacetime is regarded as a continuum with a dual quantum nature, that it curves as waves according to General Relativity while fluxing as quantum energy particles; where the latter is justified because the energy flux from early Universe plasma into space at the speed of light creating a 'spacetime continuum' or 'vacuum energy'. This concept of spacetime quantum duality can be corroborated by recent findings regarding the polarization of light from the CMB, which indicated the possible existence of an exotic substance throughout space that causes these measured polarizations [15]. By using the trace-reversed Einstein field equations, the modulus of the continuum, $E_D = (\text{stress/strain})$, is expressed as

$$E_D = \frac{T_{\mu\nu} - T g_{\mu\nu}/2}{R_{\mu\nu}/\mathcal{R}} = \frac{c^4}{8\pi G_t r_t^2} \quad (1)$$

where the stress is signified by the stress-energy tensor, $T_{\mu\nu}$, of trace, T , while the strain is signified by the Ricci curvature tensor, $R_{\mu\nu}$, as the change in curvature divided by $\mathcal{R} = 1/r_t^2$, the scalar of the pre-existing curvature, r_t is the Universe's radius of curvature and $g_{\mu\nu}$ is the metric tensor. According to the theory of elasticity, E_D is a constant; therefore, Eq. (1) shows an inverse proportionality between the gravitational 'constant', G_t , and r_t , where G_t follows the inverse square law with respect to the Universe's radius as a function of cosmic time. This relationship

is consistent with Mach's principle, the reliance of the small structure on the larger structure. Schrödinger in 1925 pointed to the reliance of G_t on the distribution of Universe's masses and the Universe's radius while Dirac in 1938 proposed its correlation to the age of the Universe [16]. The evolution in G_t can be endorsed by the measured gradual evolution in the fine-structure 'constant' [17–19], which can reveal that the presumed fundamental constants may rely on other properties of the Universe.

On the other hand, E_D is in terms of energy density and represents the continuum's resistance to deformation [20]. Eq. (1) shows E_D is proportional to the fourth-power of the speed of light, which, in turn directly proportional to the frequency; in accordance with the frequency cut-off predictions of the vacuum energy density in the Quantum Field Theory [21]; thus, E_D can characterize space-time continuum's resistance to curvature and could represent vacuum energy density. Further, the inverse proportionality in Eq. (1) could explain galaxy formation without involving dark matter where G_t was larger in value at the early Universe. Galaxy formation has been simulated using modified Newtonian gravity [22].

By incorporating the pre-existing/background curvature as a function of cosmic time and complying with the law of energy conservation, the Einstein-Hilbert action can be extended to

$$S = \int \left[\frac{E_D R}{2\mathcal{R}} + \mathcal{L}_M \right] \sqrt{-g} d^4x \quad (2)$$

where R and \mathcal{R} are the Ricci and the pre-existing scalar curvatures respectively, \mathcal{L}_M is the Lagrangian density and g is the determinant of the metric g_{uv} . The indistinctive variation in the action yields

$$\delta S = \int \left(\left[\frac{E_D}{2} \left(\frac{\delta R \sqrt{-g}}{\mathcal{R}} - \frac{\delta \mathcal{R} \sqrt{-g} R}{\mathcal{R}^2} + \frac{\delta \sqrt{-g} R}{\mathcal{R}} \right) \right] d^4x \right. \\ \left. + \left[\delta \mathcal{L}_M \sqrt{-g} + \delta \sqrt{-g} \mathcal{L}_M \right] d^4x \right) \quad (3)$$

By differentiating the determinant according to the Jacobi's formula as $\delta \sqrt{-g} = -\sqrt{-g} g_{\mu\nu} \delta g^{\mu\nu}/2$ where the variation in the metric times the inverse metric, $g^{\mu\nu} g_{\mu\nu} = \delta_\nu^\mu$, yields $g^{\mu\nu} \delta g_{\mu\nu} + g_{\mu\nu} \delta g^{\mu\nu} = 0$, while the variation in the scalar curvature, $R = R_{\mu\nu} g^{\mu\nu}$, is $\delta R = R_{\mu\nu} \delta g^{\mu\nu} + g^{\mu\nu} \delta R_{\mu\nu}$ [23]. Thus, Eq. (3) is expressed as

$$\delta S = \int \left(\left[\frac{E_D}{2\mathcal{R}} (R_{\mu\nu} \delta g^{\mu\nu} + g^{\mu\nu} \delta R_{\mu\nu}) \right] \sqrt{-g} d^4x \right. \\ \left. - \left[\frac{E_D R}{2\mathcal{R}^2} (\mathcal{R}_{\mu\nu} \delta g^{\mu\nu} + g^{\mu\nu} \delta \mathcal{R}_{\mu\nu}) \right] \sqrt{-g} d^4x \right. \\ \left. - \left[\frac{E_D R}{4\mathcal{R}} g_{\mu\nu} \delta g^{\mu\nu} \right] \sqrt{-g} d^4x \right. \\ \left. + \left[\delta \mathcal{L}_M - \frac{\mathcal{L}_M}{2} g_{\mu\nu} \delta g^{\mu\nu} \right] \sqrt{-g} d^4x \right) \quad (4)$$

The lambda/pressure is not considered, which could be implicitly incorporated into stress-energy tensors.

By considering the first boundary term in Eq. (4):

$$\int \frac{E_D}{2\mathcal{R}} g^{\mu\nu} \delta R_{\mu\nu} \sqrt{-g} d^4x \quad (5)$$

The variation in the Ricci curvature tensor $\delta R_{\mu\nu}$ can be written in terms of the covariant derivative of the difference between two Levi-Civita connections, the Palatini identity:

$$\delta R_{\mu\nu} = \nabla_\rho (\delta \Gamma_{\mu\nu}^\rho) - \nabla_\nu (\delta \Gamma_{\mu\rho}^\rho) \quad (6)$$

The variation in the Ricci curvature tensor with respect to the inverse metric $g^{\mu\nu}$ can be obtained by utilising the metric compatibility of the covariant derivative, $\nabla_\rho g^{\mu\nu} = 0$ [23] as

$$g^{\mu\nu} \delta R_{\mu\nu} = \nabla_\rho (g^{\mu\nu} \delta \Gamma_{\mu\nu}^\rho) - \nabla_\nu (g^{\mu\nu} \delta \Gamma_{\mu\rho}^\rho) \quad (7)$$

By substituting Eq.(7) to Eq. (5), the boundary term as a total derivative for any tensor density can be transformed according to the Stokes' theorem with renaming the dummy indices as

$$\begin{aligned} \frac{E_D}{2\mathcal{R}} \int \nabla_\mu (g^{\sigma\nu} \delta \Gamma_{\nu\sigma}^\mu - g^{\sigma\mu} \delta \Gamma_{\mu\sigma}^\nu) \sqrt{-g} d^4x &\equiv \frac{E_D}{2\mathcal{R}} \iiint_V \nabla_\mu A^\mu \sqrt{-g} dV \\ &= \frac{E_D}{2\mathcal{R}} \iint_S A^\mu \cdot \hat{n}_\mu \sqrt{|q|} dS = \frac{E_D}{2\mathcal{R}} \oint_{\partial V} K \epsilon \sqrt{|q|} d^3x \end{aligned} \quad (8)$$

The non-boundary term $E_D/2\mathcal{R}$ is left outside the integral transformation as it only acts as a scalar to the integral that called S_{GHY} [24]. K is the trace of the extrinsic curvature tensor, q is the determinant of the induced metric and ϵ equals 1 when the normal \hat{n}_μ is a spacelike entity and equals -1 when it is a timelike entity. By substituting Eq. (8) to Eq. (4):

$$\delta S = \int \left(\begin{aligned} &+ \left[\frac{E_D}{2\mathcal{R}} R_{\mu\nu} \right] \sqrt{-g} d^4x \delta g^{\mu\nu} \\ &+ \left[\frac{E_D \epsilon}{2\mathcal{R}} K \right] \sqrt{|q|} d^3x \\ &- \left[\frac{E_D R}{2\mathcal{R}^2} \mathcal{R}_{\mu\nu} \right] \sqrt{-g} d^4x \delta g^{\mu\nu} \\ &- \left[\frac{E_D R \epsilon}{2\mathcal{R}^2} K \right] \sqrt{|q|} d^3x \\ &- \left[\frac{E_D R}{4\mathcal{R}} g_{\mu\nu} \right] \sqrt{-g} d^4x \delta g^{\mu\nu} \\ &+ \left[\frac{\delta \mathcal{L}_M}{\delta g^{\mu\nu}} - \frac{\mathcal{L}_M}{2} g_{\mu\nu} \right] \sqrt{-g} d^4x \delta g^{\mu\nu} \end{aligned} \right) \quad (9)$$

It is worth noting that some terms satisfy the criteria that the variation in the action δS is with respect to the variation in their inverse metric $\delta g^{\mu\nu}$ excluding the boundary terms that still lack this feature. To achieve the consistency of the action, the variation in the boundary action has to be determined. Thus, the indistinctive variation in the first boundary term is

$$\frac{E_D \epsilon}{2\mathcal{R}} \int \left(K_{\mu\nu} \delta q^{\mu\nu} + q^{\mu\nu} \delta K_{\mu\nu} + K \frac{\delta \sqrt{|q|}}{\sqrt{|q|}} \right) \sqrt{|q|} d^3x \quad (10)$$

where $K = K_{\mu\nu} q^{\mu\nu}$. $K_{\mu\nu}$ is the extrinsic curvature tensor and $q_{\mu\nu}$ is the induced metric on the boundary. The non-boundary term $E_D \epsilon / 2\mathcal{R}$ is left outside, where it

can be considered as a scalar. Otherwise, its variational terms can be incorporated in the conformal transformation function Ω^2 as follows. By utilizing Jacobi's formula for the determinant differentiation as $\delta \sqrt{|q|} = -\sqrt{|q|} q_{\mu\nu} \delta q^{\mu\nu} / 2$; and the variation in $q^{\mu\nu} q_{\mu\nu} = \delta_\nu^\mu$ as $q^{\mu\nu} = -q_{\mu\nu} \delta q^{\mu\nu} / \delta q_{\mu\nu}$; Therefore, Eq. (10) can be expressed as

$$\frac{E_D \epsilon}{2\mathcal{R}} \int \left(K_{\mu\nu} - \frac{K}{2} \left(q_{\mu\nu} + 2q_{\mu\nu} \frac{\delta K_{\mu\nu}}{\delta q_{\mu\nu} K} \right) \right) \sqrt{|q|} d^3x \delta q^{\mu\nu} \quad (11)$$

here $\delta K_{\mu\nu} / \delta q_{\mu\nu} K = (\delta K_{\mu\nu} / K_{\mu\nu}) (q_{\mu\nu} / \delta q_{\mu\nu}) = \delta \ln K_{\mu\nu} / \delta \ln q_{\mu\nu}$ can resemble the Ricci flow in a normalised form reflecting the conformal distortion in the boundary, which can be expressed as a positive function Ω^2 based on Weyl's conformal transformation [25] as $\bar{q}_{\mu\nu} = q_{\mu\nu} \Omega^2$. Therefore, Eq. (11) is written as

$$\frac{E_D \epsilon}{2\mathcal{R}} \int \left(K_{\mu\nu} - \frac{1}{2} K \hat{q}_{\mu\nu} \right) \sqrt{|q|} d^3x \delta q^{\mu\nu} \quad (12)$$

where $\hat{q}_{\mu\nu} = q_{\mu\nu} + 2\bar{q}_{\mu\nu}$ is the conformal transformation of the induced metric where Einstein spaces are a subclass of the conformal space [26]. The same is applied for the second boundary term. Thus, the action in Eq. (9) is rewritten as

$$\delta S = \int \left(\begin{aligned} &+ \left[\frac{E_D}{2\mathcal{R}} R_{\mu\nu} \right] \sqrt{-g} d^4x \delta g^{\mu\nu} \\ &+ \left[\frac{E_D \epsilon}{2\mathcal{R}} \left(K_{\mu\nu} - \frac{1}{2} K \hat{q}_{\mu\nu} \right) \right] \sqrt{|q|} d^3x \delta q^{\mu\nu} \\ &- \left[\frac{E_D R}{2\mathcal{R}^2} \mathcal{R}_{\mu\nu} \right] \sqrt{-g} d^4x \delta g^{\mu\nu} \\ &- \left[\frac{E_D R \epsilon}{2\mathcal{R}^2} \left(K_{\mu\nu} - \frac{1}{2} K \hat{q}_{\mu\nu} \right) \right] \sqrt{|q|} d^3x \delta q^{\mu\nu} \\ &- \left[\frac{E_D R}{4\mathcal{R}} g_{\mu\nu} \right] \sqrt{-g} d^4x \delta g^{\mu\nu} \\ &+ \left[\frac{\delta \mathcal{L}_M}{\delta g^{\mu\nu}} - \frac{\mathcal{L}_M}{2} g_{\mu\nu} \right] \sqrt{-g} d^4x \delta g^{\mu\nu} \end{aligned} \right) \quad (13)$$

The stress-energy tensor is proportional to the Lagrangian term by definition [23] as

$$T_{\mu\nu} := \mathcal{L}_M g_{\mu\nu} - 2 \frac{\delta \mathcal{L}_M}{\delta g^{\mu\nu}} \quad (14)$$

By substituting Eq.(14) in Eq. (13), choosing ϵ as a timelike entity and then applying the principle of stationary action yield

$$\frac{R_{\mu\nu}}{\mathcal{R}} - \frac{K_{\mu\nu} - \frac{K \hat{q}_{\mu\nu}}{2}}{\mathcal{R}} - \frac{R \mathcal{R}_{\mu\nu}}{\mathcal{R}^2} + R \frac{K_{\mu\nu} - \frac{K \hat{q}_{\mu\nu}}{2}}{\mathcal{R}^2} - \frac{R g_{\mu\nu}}{2\mathcal{R}} = \frac{T_{\mu\nu}}{E_D} \quad (15)$$

Eqs. (15) can be rearranged as

$$\frac{\mathcal{R} R_{\mu\nu} - R \mathcal{R}_{\mu\nu}}{\mathcal{R}^2} - \frac{R}{2\mathcal{R}} g_{\mu\nu} + \frac{R - \mathcal{R}}{\mathcal{R}^2} \left(K_{\mu\nu} - \frac{1}{2} K \hat{q}_{\mu\nu} \right) = \frac{T_{\mu\nu}}{E_D} \quad (16)$$

since $\mathcal{R}_{\mu\nu} / \mathcal{R} = \mathcal{R}_{\mu\nu} / \mathcal{R}_{\mu\nu} \bar{g}^{\mu\nu} = \bar{g}_{\mu\nu}$ corresponds to Weyl's conformal transformation of the metric [25,26], where the conformal transformation can describe the tidal distortion and the gravitational waves in the absence of matter [27], and by using a conformally transformed metric, $\hat{g}_{\mu\nu} = g_{\mu\nu} + 2\bar{g}_{\mu\nu}$, and rearranging Eqs. (16),

the extended field equations are

$$\frac{R_{\mu\nu}}{\mathcal{R}} - \frac{1}{2}\mathcal{R}\hat{g}_{\mu\nu} + \frac{R-\mathcal{R}}{\mathcal{R}^2}\left(K_{\mu\nu} - \frac{1}{2}K\hat{q}_{\mu\nu}\right) = \frac{T_{\mu\nu}}{E_D} \quad (17)$$

Eqs. (17) can be interpreted as indicating that the induced curvature over the pre-existing curvature equals the ratio of the imposed energy density and its flux to the vacuum energy density and its flux through an expanding/contracting Universe. They can be simplified by substituting Eq. (1) to Eqs. (17) as

$$R_{\mu\nu} - \frac{1}{2}\mathcal{R}\hat{g}_{\mu\nu} + \frac{R-\mathcal{R}}{\mathcal{R}}\left(K_{\mu\nu} - \frac{1}{2}K\hat{q}_{\mu\nu}\right) = \frac{8\pi G_t}{c^4}T_{\mu\nu} \quad (18)$$

The new boundary tensor/term is only significant at high-energy limits such as within black holes [24] and the early Universe, and could remove the singularities and satisfy a conformal invariance theory. The evolution in G_t can accommodate the pre-existing curvature, \mathcal{R} , evolution over cosmic time, t , against the constant G for the special flat space-time case.

3. Bounce from a Closed Early Universe

3.1 Early Universe Plasma Model

The Friedmann–Lemaître–Robertson–Walker (FLRW) metric is the standard cosmological metric model, which assumes an isotropic and homogenous Universe [28,29], where the isotropy and homogeneity of the early Universe plasma based on the CMB are consistent with this metric model. The PL18 release revealed a closed early Universe. Thus, the plasma reference radius of curvature r_p upon the emission of the CMB and the corresponding early Universe scale factor a_p at the reference cosmic time t_p are incorporated in order to reference the metric as shown in Figure 1. Hence, the referenced metric is

$$ds^2 = c^2 dt^2 - \frac{a^2}{a_p^2} \left(\frac{dr^2}{1 - \frac{r^2}{r_p^2}} + r^2 d\theta^2 + r^2 \sin^2\theta d\phi^2 \right) \quad (19)$$

where a/a_p is a new dimensionless scale factor. No conformal distortion is included in this metric, thus, its outcomes are comparable with the literature. The Ricci curvature tensor and Ricci scalar curvature are solved using Christoffel symbols of the second kind for g_{uv} in Eqs. (19) (derivations in Appendix A) as

$$R_{tt} = -3\frac{\ddot{a}}{a}, \quad R_{\theta\theta} = \frac{r^2}{c^2} \left(\frac{a\ddot{a}}{a_p^2} + \frac{2\dot{a}^2}{a_p^2} + \frac{2c^2}{r_p^2} \right), \quad (20)$$

$$R_{rr} = \frac{1}{c^2} \left(\frac{a\ddot{a}}{a_p^2} + \frac{2\dot{a}^2}{a_p^2} + \frac{2c^2}{r_p^2} \right) / \left(1 - \frac{r^2}{r_p^2} \right),$$

$$R_{\phi\phi} = \frac{r^2 \sin^2\theta}{c^2} \left(\frac{a\ddot{a}}{a_p^2} + \frac{2\dot{a}^2}{a_p^2} + \frac{2c^2}{r_p^2} \right).$$

$$R = R_{\mu\nu}g^{\mu\nu} = \frac{-6}{c^2} \left(\frac{\ddot{a}}{a} + \frac{\dot{a}^2}{a^2} + \frac{c^2 a_p^2}{a^2 r_p^2} \right). \quad (21)$$

where the dot represents a cosmic time derivative.

Figure 1 shows the referenced metric model of the early Universe plasma expansion.

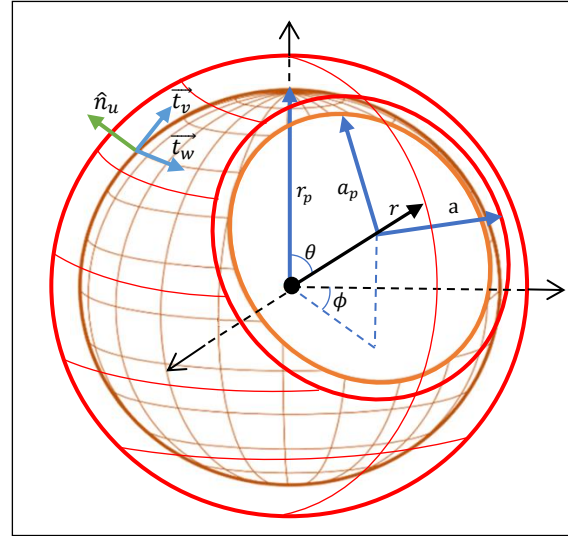


Figure 1. The hypersphere of a positively curved early Universe plasma expansion upon the CMB emissions. r_p is the reference radius of the intrinsic curvature and a_p is the corresponding reference scale factor of the early Universe at reference cosmic time t_p while \hat{n}_u and \vec{t}_v are the normal and tangential vectors on the manifold boundary respectively regarding the extrinsic curvature.

3.2 Universe Evolution Model

By solving the field equations for a perfect fluid given by $T_{\mu\nu} = (\rho + P/c^2)u_\mu u_\nu + P g_{\mu\nu}$ [30] and substituting Eqs. (19-21), the Friedmann equations that count for the plasma reference radius and reference scale factor are

$$H^2 \equiv \frac{\dot{a}^2}{a^2} = \frac{8\pi G_t \rho}{3} - \frac{c^2 a_p^2}{a^2 r_p^2}, \quad (22)$$

$$\dot{H} \equiv \frac{\ddot{a}}{a} = -\frac{4\pi G_t}{3} \left(\rho + 3\frac{P}{c^2} \right). \quad (23)$$

where H , P , and ρ are Hubble parameter, pressure, and density respectively.

By utilizing the imaginary cosmic time, $\tau = it$, the referenced Friedman equations in Eqs. (22, 23) are solved over conformal time by rewriting Eq. (22) in terms of the conformal time in its parametric form, $d\eta = -i\frac{a_p}{a}d\tau$ (where $\dot{a} = i\frac{da}{d\tau}$); thus, $d\eta = \frac{a_p}{aa}da$ as

$$\int_0^\eta d\eta = \int_0^{2\pi} a_p \left(\frac{8\pi G_p \rho_p a_p^3}{3} a - \frac{c^2 a_p^2}{r_p^2} a^2 \right)^{-1/2} da \quad (24)$$

where $\rho = \frac{\rho_p a_p^3}{a^3}$ [31]. By integrating, the evolution of the scale factor is

$$a(\eta)/a_p = \frac{M_p G_p}{c^2 r_p} \left(1 - \cos \frac{c}{r_p} \eta \right) \quad (25)$$

where $M_p = \frac{4}{3}\pi\rho_p r_p^3$ is the plasma mass and G_p is the gravitational parameter value at τ_p .

The constant in Eq. (25) can be rewritten in terms of the modulus E_D representing the vacuum energy density and the Universe energy density E by using Eq. (1) as $E/6E_D$. Additionally, the evolution of the imaginary time $\tau(\eta)$ can be obtained by integrating the length of the spatial factor contour over the expansion speed H_η while initiating at the reference imaginary time τ_p with the corresponding scale factor a_p . Therefore, by rewriting Eq. (25) in terms of the Hubble parameter by its definition and initiating at τ_p as $d\tau = i \frac{da(\eta)}{H_\eta a_p}$:

$$\int_{\tau_p}^{\tau} d\tau = i \int_0^\eta \frac{E}{6H_\eta E_D} \left(1 - \cos \frac{c}{r_p} \eta\right) d\eta \quad (26)$$

By integration, the evolution of imaginary time is

$$\tau(\eta) = i \frac{E}{6H_\eta E_D} \left(\eta - \sin \frac{c}{r_0} \eta\right) + \tau_p \quad (27)$$

According to the law of energy conservation, the divergence of the stress-energy tensor vanishes, $\Delta_\nu T^{\nu\mu}$, thus, $\frac{a}{a} T^u_u + 3 \frac{a}{a} \rho - i \frac{\partial \rho}{\partial \tau} = 0$, $3 \left(\rho + \frac{P}{c^2}\right) \frac{a}{a} - i \frac{\partial \rho}{\partial \tau} = 0$. By combining these outcomes, integrating, and substituting the spatial scale factor rate in Eq. (25) to their outcome, the density evolution of matter is

$$\rho_{\eta,m} = D_p \left(1 - \cos \frac{c}{r_p} \eta\right)^{-3} \quad (28)$$

where D_p is constant. According to Eq. (23), the rate of Hubble parameter, \dot{H} , relies on the density; thus, by substituting Eqs. (28) to Eq. (23):

$$\dot{H} \equiv \frac{\ddot{a}}{a} = -\frac{4\pi G_t}{3} D_p \left(1 - \cos \frac{c}{r_p} \eta\right)^{-3} \quad (29)$$

By substituting Eq. (25) to Eq. (29) and rewriting them in terms of Hubble parameter rate \dot{H}_η by its definition and initiating the integration at τ_p as $\int \dot{H} = \int \ddot{a}/a_p$ as

$$H_{\eta,m} = H_m \left(\frac{1}{3} \cot^3 \frac{c}{2r_p} \eta + \cot \frac{c}{2r_p} \eta\right) + H_p \quad (30)$$

Similarly, by applying the same procedure for the radiation-only density evolution, Hubble parameter evolution for radiation-only is

$$H_{\eta,r} = H_r \left(\frac{1}{5} \cot^5 \frac{c}{2r_p} \eta + \frac{2}{3} \cot^3 \frac{c}{2r_p} \eta + \cot \frac{c}{2r_p} \eta\right) + H_p \quad (31)$$

where H_m, H_r and H_p are constants. The quantized wave function ψ_L with respect to its reference value ψ_p at τ_p is obtained by using Eqs. (25, 27-31) as a potential third quantization as

$$\psi_L(\eta)/\psi_p = \mp \frac{E}{6E_D} \left(\left(1 - \cos \frac{c}{r_p} \eta\right)^i + \frac{c^2}{H_\eta^2 a_p^2} \left(\eta - \sin \frac{c}{r_p} \eta\right)^{2i}\right)^{1/2} e^{i \cot^{-1} \frac{|H_\eta| a_p (1 - \cos \frac{c}{r_p} \eta)}{c \left(\eta - \sin \frac{c}{r_p} \eta\right)}} \quad (32)$$

here E/E_D is a new dimensionless energy density parameter as the ratio of the Universe energy density to the vacuum energy density.

3.3 Plasma Boundary Contribution

For high energy limits, the gravitational contribution of the plasma boundary can be obtained using the boundary term, $\frac{R-R}{R} (K_{\mu\nu} - \frac{1}{2} K q_{\mu\nu}) = \frac{8\pi G_t}{c^4} T_{\mu\nu}$, where at τ_p , there is no conformal transformation. Therefore, the induced metric tensor on the plasma hypersphere boundary $q_{\mu\nu}$ [32] is

$$[q_{\mu\nu}] = \text{diag} \left(-c^2, \frac{a^2(t)}{a_p^2} R^2, \frac{a^2(t)}{a_p^2} R^2 \sin^2 \theta\right) \quad (33)$$

The extrinsic curvature tensor is solved utilizing the formula $K_{uv} = -\vec{t}_\mu \cdot \nabla_\nu \hat{n}_v$. Due to the hypersphere smoothness, the covariant derivative reduces to partial derivative as $K_{uv} = -\vec{t}_\mu \partial \hat{n} / \partial \bar{t}^\nu$ [32]; thus:

$$[K_{\mu\nu}] = \text{diag} \left(0, -\frac{a^2(t)}{a_p^2} R, -\frac{a^2(t)}{a_p^2} R \sin^2 \theta\right) \quad (34)$$

The trace of the extrinsic curvature is $K = K_{\mu\nu} q^{\mu\nu} = -2/R = -2/r_p^2$. The pre-existing curvature of the plasma boundary at τ_p is $\mathcal{R}_p = 1/r_p^2$ (Gaussian curvature). On the other hand, the Ricci scalar curvature can be written as the difference between the kinetic and potential energy densities whereby substituting Friedmann equations in Eqs. (22, 23) to the Ricci scalar curvature in Eqs. (21) at τ_p as

$$R_p = G_p \left(\frac{24\pi P_p}{c^4} - \frac{8\pi \rho_p}{c^2}\right) \quad (35)$$

By solving the boundary for a perfect fluid given by $T_{\mu\nu} = (\rho + P/c^2) u_\mu u_\nu + P g_{\mu\nu}$ and substituting Eqs. (35-33) into the boundary term as

$$\frac{G_p \left(\frac{24\pi P_p}{c^4} - \frac{8\pi \rho_p}{c^2}\right) - \frac{1}{r_p^2} \left(-c^2\right)}{1/r_p^2} = 8\pi G_p \rho_p \quad (36)$$

By multiplying by both sides by plasma volume V_p :

$$\tau_p = \frac{4G_p P_p V_p}{c^4} \quad (37)$$

The reference radius $r_p > 0$ because any reduction in plasma volume causes an increase in its pressure.

4. Universe Evolution

The positive and negative solutions of the wave function ψ_L imply that matter and antimatter in the plasma evolved in opposite directions. The evolution of the Universe according to the wave function for both matter and radiation-only in addition to the light cone are shown in Figure 2a; where only the positive solution of one Universe side is shown due to their symmetry. A chosen mean evolution value of the Hubble parameter of $\sim 70 \text{ km}\cdot\text{s}^{-1}\cdot\text{Mpc}^{-1}$ and a phase transition of expansion at age of $\sim 10 \text{ Gyr}$ were applied to tune the integration constants of the model; accordingly, the predicted energy density parameter is ~ 1.16 . Further, the Hubble parameter evolution and its rate are shown in Figure 2b.

According to the wave function (Figure 2a, orange curve), the cosmic evolution can be interpreted as comprising three distinct phases. Firstly, matter and antimatter sides of the Universe expanded in opposite directions away from the early plasma during the first phase perhaps due to the phenomenon of plasma drift in the presence of electromagnetic fields where

the expansion speed shown in Figure 2b (blue curve, Hubble parameter) starts with a hyperbolic rate at the nascent stage, then, the rate decreases due to gravity between the two sides, until it reached its minimal value at the phase transition at age of ~ 10 Gyr. The evolution in Hubble parameter is evidence from three time-delay cosmography observations [33].

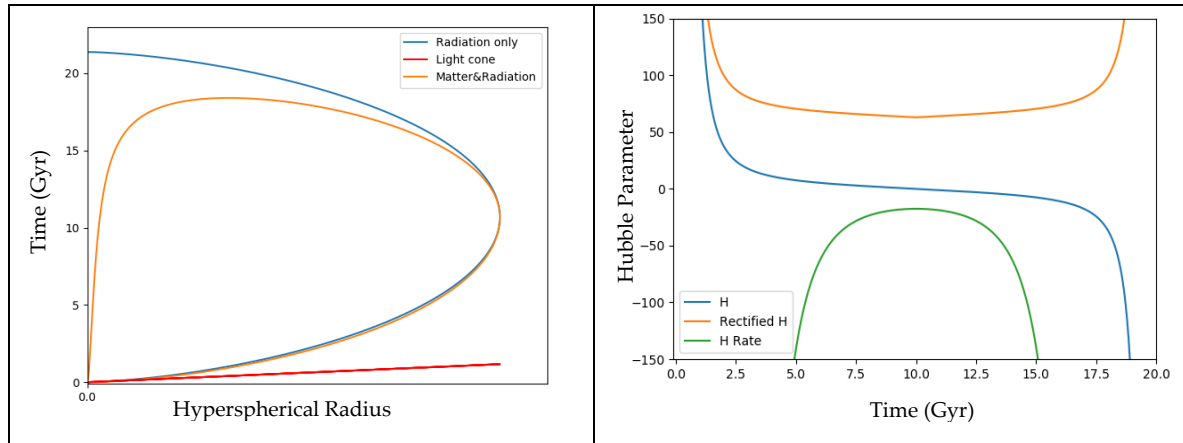


Figure 2. A) Evolution of the wave function of matter of one side of the Universe, radiation only wave function in addition to the straight line of light cone (diagram is not to scale). B) The evolution of the Hubble parameter H and its rate \dot{H} in addition to a rectified Hubble parameter reflecting the reverse expansion direction.

However, the wave function reverses its direction in the second phase with both sides of matter and antimatter entering a state of free-fall towards each other at gravitational acceleration possibly causing current accelerated expansion; the Hubble parameter starts to increase in the reverse direction.

According to mechanics, the minus sign of the speed indicates an opposite direction while the opposite signs of the acceleration (Figure 2b, green curve) and the speed in the first phase indicate a slowing down while the matching signs in the second phase indicate the speed of expansion is increasing.

A congruence of space-time worldlines has been simulated to virtualize the matter wave function (Figure 3a). In the first phase, the simulation of the worldlines produced a curved geometry in harmony with the PL18 [5,6]. Conversely, for the accelerated present phase in reverse directions, the simulation of the worldlines produced a flat end or flat space-time, explaining current space-time flatness. The apparent Universe's topology due to the gravitational lensing effects is shown in Figure 3b, possibility matching the large-angle correlations of the CMB [34] and the SLOAN Digital Sky Survey data virtualization [35].

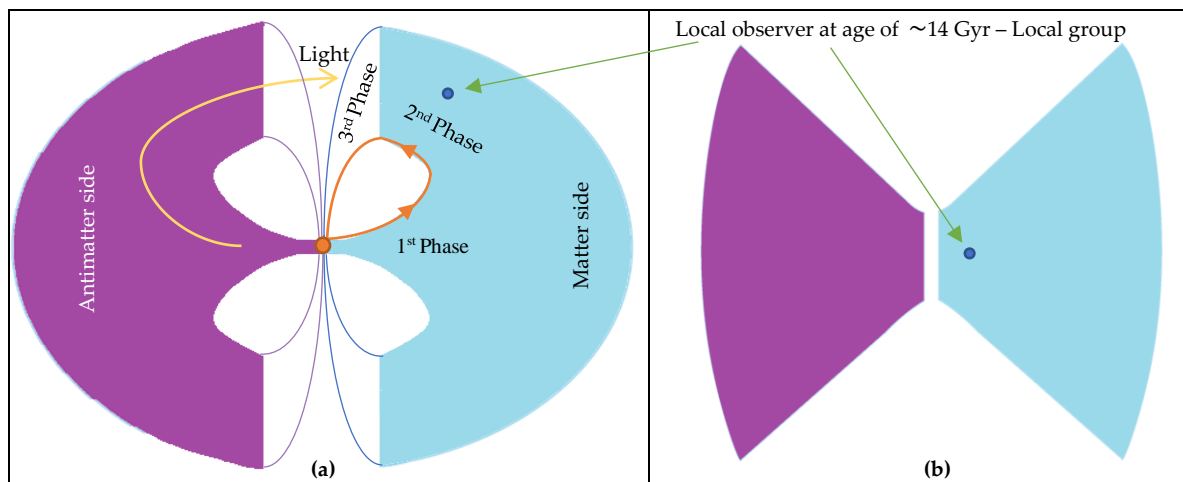


Figure 3. A) The predicted cosmic topology of both sides. Firstly, a decelerated phase of both sides away from early Universe plasma; secondly, an accelerated phase in reverse directions where both sides free fall toward each other under gravitational acceleration. Finally, a rapid contraction phase leading to a Big Crunch. B) The apparent topology due to the gravitational lensing effects.

In addition, this reasoning for current accelerated expansion, due to the free-fall of both sides towards each other under gravitational acceleration, can also explain the observed dark flow towards the great attractor that cannot be observed [36]. Further, the observed strong “dipole repeller” [37] can endorse this model; the authors argued their observation is incompatible with an attractive gravitational force while the under-dense and over-dense regions explanation for this phenomenon seems incomplete as accordingly numerous regions that differently dense create multiple weak attractors-repellers throughout the Universe. On the other hand, since our local group (Figure 3a, blue dot at age of ~ 14 Gyr) flows in a direction towards the antimatter side while the corresponding galaxy group in the antimatter side flows in a direction towards our group. Therefore, the flow of the matter side including our group can signify the great attractor while the flow of the antimatter side towards our group can signify the corresponding repeller.

Further, since at the second phase both sides move closer to each other; this would increase the average density, which can explain the reason of the current increase in the average temperature of the Universe [38] in contrast to the state of cooling down from hot plasma during the first phase.

Furthermore, the measured gradual evolution in the fine structure ‘constant’, where its observed variation occurs both with time and across a specific axis [17], could evolve along with the evolution of the matter wave function that effects the average density.

Interestingly, the matter wave function predicts a final phase of spatial contraction that appears after ~ 18 Gyr, which could be because of the future high concentration of matter/antimatter at both sides, leading to a Big Crunch. On the other hand, the radiation-only according to its wave function, which propagates faster than matter, is predicted to pass from a side to other side (Figure 2a, blue curve), which could explain why CMB light can be observed even though matter moves much slowly than light.

Figure 4 shows 3D spatial and 1D temporal dimensions schematic of the space-time evolutions of both sides, which can be in correspondence with the Kaluza–Klein unified theory. Due to the anisotropy in the expansion of the early Universe hypersphere into two sides, the expansion in time and hence the time dimension can be analysed and considered as two dimensions, the imaginary (future-past) and the real (forward-backward) time components. Thus, the fifth dimension would be the real time component while the cylindrical condition belongs to the scale factor; antimatter travels backwards in real time.

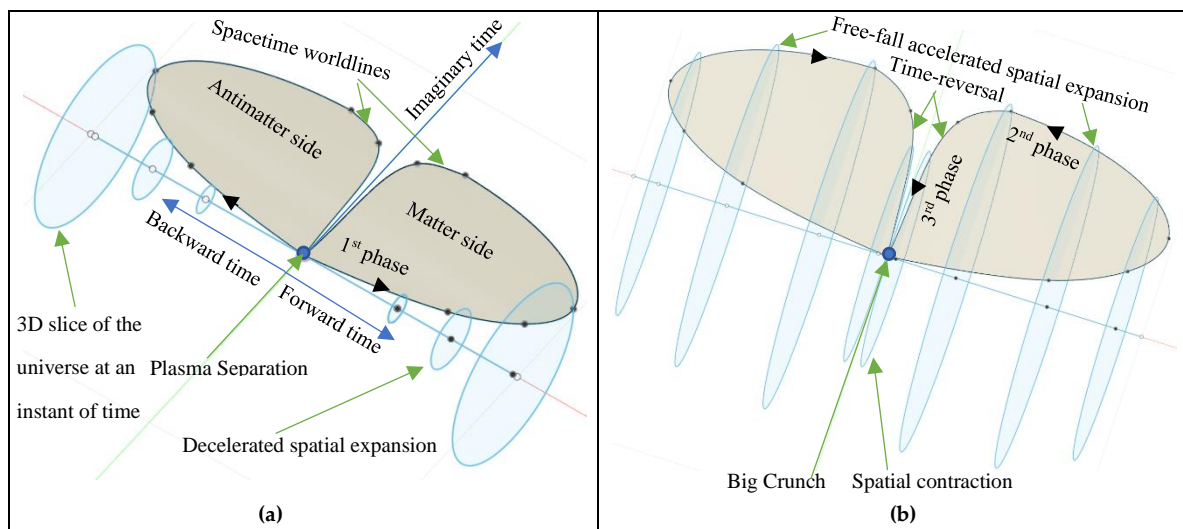


Figure 4. **A)** Schematic in 3D spatial and 1D temporal dimensions of both sides, according to the space-time worldline evolution. **(a)** In the first phase, both sides expand away from the early plasma. **(b)** In the second phase, both sides expand in reverse directions and free-fall towards each other at gravitational acceleration. In the third phase, both sides contract, due to high concentrations of matter/antimatter, leading to the Big Crunch. Blue circles represent a 3D Universe slice, which is not necessarily a simply path connected.

The inverse square law of G_t with respect to the Universe’s radius could explain the galaxy formation without involving dark matter where G_t was larger in value at the early Universe. This could explain the gravity hierarchy problem while for a proper comp-

lete cycle of the wave function, the minimal radius is equal the distance that light travels in one second in free space, which may hint the origin of the speed value. Moreover, the model can be consistence with galaxy rotation curve as discussed in the next section.

5. Simulation of a Spiral Galaxy

The consistent patterns of galactic rotation curves observed using precise and independent galactic redshift data have confirmed that hydrogen clouds and outermost stars are orbiting galaxies at speeds faster than those calculated using Newtonian laws. Accordingly, the dark matter hypothesis was introduced to account for the apparently missing galactic mass and explain these fast-orbital velocities [39,40]. However, no evidence for the existence of dark matter, which is hypothesized to account for the majority of galactic mass, has been observed since its introduction. The failure to find dark matter led to the introduction of new theories such as modified gravity and MOND [41–45]. Several recent studies have reported that many galaxies do not contain dark matter [46]. This scenario was used to inform galaxy formation simulations using modified Newtonian dynamics without considering the effects of dark matter [22]. In addition, external fields that influence galactic rotation speeds were detected at up to 8σ to 11σ , which challenge traditional dark matter concepts [11]. Therefore, there is no evidence for the existence or nature of dark matter.

Alternatively, the curvature of the space-time continuum is predicted to change over the age of the Universe, that is, a conformal curvature evolution is expected, with the highest degree of curvature occurring at the phase transition as determined by the derived wave function (see Figure 3a). Accordingly, it can be inferred that the fast orbital speeds observed for outer stars in galaxies are a result of their travel through conformally curved space-time.

To evaluate this inference, a fluid dynamics simulation was performed based on Newtonian dynamics using the Fluid Pressure and Flow software [47]. In this simulation, the fluid was deemed to represent the space-time continuum that flows throughout an incrementally flattening curvature paths. Using these conditions, a fluid model was built to analyse the external momenta exerted on objects flowing along an incrementally flattening curvature, which represents the conformal curvature evolution as shown in Figure 5a. The momenta yielded by the fluid modelling were used to inform a simulation of a spiral galaxy as a forced vortex (under external fields), as shown in Figure 5b.

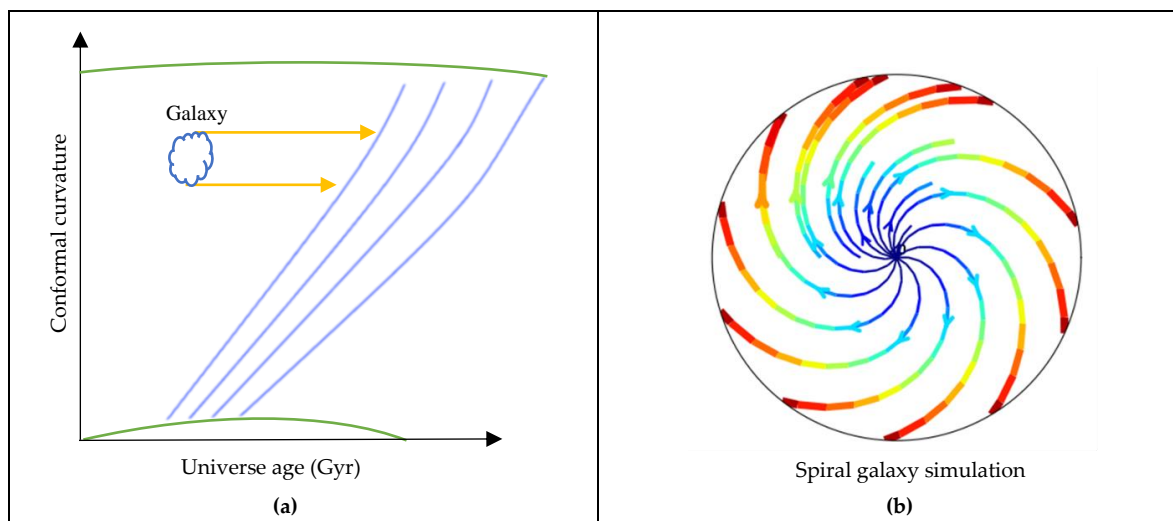


Figure 5. A) External momenta exerted on a galaxy due to its travel through a conformally curved space-time. Green curves represent an incrementally flattening conformal curvature of space-time worldlines. Blue curves show the resultant external fields exerted on galaxies. B) Simulation of spiral galaxy rotation. Blue represents the slowest tangential speeds, and red represents the fastest speeds.

The simulation shows that the tangential speeds of outer parts of the spiral galaxy are rotating faster in comparison with the rotational speeds of inner parts. Additionally, the galaxies of the same mass in the present Universe would rotate faster than they were in the past because of the increase in the external momenta due to the highest conformal curvature at the phase transition. Based on these results, it can be concluded the conformal curvature is responsible for the fast orbital speed of outer stars in galaxies.

6. Conclusions and Future Works

In this study, the pre-existing curvature is incorporated to extend the field equations where a closed early Universe model is considered by utilising a referenced FLRW metric model. The evolution of the Universe from early plasma is modelled utilising the Universe wave function. The wave function revealed both positive and negative solutions implying that the Universe evolved into two opposite sides: matter and antimatter.

The derived wave function predicted that a nascent hyperbolic expansion is followed by a phase of decelerating spatial expansion during the first ~ 10 Gyr, and then, a second phase of accelerating expansion. The plasma drift in the presence of electromagnetic fields could provide a physical explanation for the expansion of the early Universe against the gravity of its early hot and very dense state; where both sides of the Universe expand away from the early plasma during the first phase. Then, during the second phase, they reverse their directions and free fall towards each other. It is conceivable that, the matter and antimatter are free-falling towards each other, causing the present accelerating expansion of the Universe. This could explain the effects attributed to dark energy as well as the observed dark flow and dipole repeller.

The radiation only worldlines which predicted to pass from one side to another could explain why CMB light can be observed even though matter moves much more slowly than light while the apparent topology is possibly in accordance with the large-angle correlations of the CMB and the SLOAN Digital Sky Survey data.

Further, the simulated spacetime worldlines during the decelerating phase were found to be flattened during the accelerating phase due to the reverse direction of the continuum worldlines, explaining the current space flatness while at the early Universe the simulation showed a positive curvature in accordance with PL18. In addition, the predicted topology could fit well the observed supervoids, galaxy filaments and walls.

Regarding the fast-orbital speed of outer stars, the simulation could provide a physical explanation by which the fast orbital speed of outer stars owing to the external fields exerted on galaxies as they travel through conformally curved space-time rather than the existence of dark matter. The inverse square law of G_t with respect to the Universe's radius could explain the galaxy formation without involving dark matter where G_t was larger at the early Universe, which could explain the gravity hierarchy problem.

The model predicted a final phase of time-reversal of spatial contraction leading to a Big Crunch, signifying a cyclic Universe. The derived smallest possible reference radius of the early plasma due to its boundary gravitational contributions can reveal that the early Universe expansion upon emission of the CMB might mark the beginning of the Universe from a previous collapse one.

Finally, this theoretical work will be tested against observational data in future works.

Funding: This research received no funding.

Acknowledgements: I am grateful to the Preprints Editor Ms Mila Marinkovic for her rapid and excellent attention in processing the submissions.

Conflicts of Interest: The author declares no conflict of interest

Appendix A

The Ricci curvature tensor R_{uv} is solved using the Christoffel symbols of the second kind given by $\Gamma_{\mu\nu}^{\rho} = \frac{1}{2}g^{\rho\lambda}(\partial_{\mu}g_{\lambda\nu} + \partial_{\nu}g_{\lambda\mu} - \partial_{\lambda}g_{\mu\nu})$ for the referenced metric tensor $g_{\mu\nu}$ in Eq. (19):

$$\Gamma^0_{11} = \frac{a\dot{a}}{c^2 a_p^2 \left(1 - \frac{r^2}{r_p^2}\right)}, \quad \Gamma^1_{11} = \frac{r}{r_p^2 \left(1 - \frac{r^2}{r_p^2}\right)}, \quad (\text{A.1})$$

$$\Gamma^0_{22} = \frac{r^2 a\dot{a}}{c^2 a_p^2}, \quad \Gamma^1_{22} = -r \left(1 - \frac{r^2}{r_p^2}\right), \quad (\text{A.2})$$

$$\Gamma^0_{33} = \frac{r^2 a\dot{a} \sin^2 \theta}{c^2 a_p^2}, \quad \Gamma^1_{33} = -r \sin^2 \theta \left(1 - \frac{r^2}{r_p^2}\right), \quad (\text{A.3})$$

$$\Gamma^1_{01} = \Gamma^2_{02} = \Gamma^3_{03} = \Gamma^1_{10} = \Gamma^2_{20} = \Gamma^3_{30} = \frac{\dot{a}}{a}, \quad (\text{A.4})$$

$$\Gamma^2_{12} = \Gamma^2_{21} = \Gamma^3_{13} = \Gamma^3_{31} = \frac{1}{r}, \quad (\text{A.5})$$

$$\Gamma^2_{33} = -\sin \theta \cos \theta, \quad \Gamma^3_{23} = \Gamma^3_{32} = \cot \theta \quad (\text{A.6})$$

The Ricci curvature tensor given by $R_{\mu\nu} = \partial_{\lambda}\Gamma^{\lambda}_{\mu\nu} - \partial_{\nu}\Gamma^{\lambda}_{\mu\lambda} + \Gamma^{\rho}_{\mu\nu}\Gamma^{\lambda}_{\rho\lambda} - \Gamma^{\rho}_{\mu\lambda}\Gamma^{\lambda}_{\rho\nu}$. The $t-t$ component of the Ricci tensor is

$$R_{tt} = R_{00} = -\partial_0\Gamma^1_{01} - \partial_0\Gamma^2_{02} - \partial_0\Gamma^3_{03} - \Gamma^1_{01}\Gamma^1_{10} - \Gamma^2_{02}\Gamma^2_{20} - \Gamma^3_{03}\Gamma^3_{30} \quad (\text{A.7})$$

$$R_{tt} = -3\partial_t \frac{\dot{a}}{a} - 3\left(\frac{\dot{a}}{a}\right)^2 = -3\frac{\ddot{a}a - \dot{a}^2}{a^2} - 3\frac{\dot{a}^2}{a^2} = -3\frac{\ddot{a}}{a} \quad (\text{A.8})$$

The $r-r$ component

$$R_{rr} = R_{11} = \partial_0\Gamma^0_{11} - \partial_1\Gamma^2_{12} - \partial_1\Gamma^3_{13} + \Gamma^0_{11}\Gamma^2_{02} + \Gamma^0_{11}\Gamma^3_{03} - \Gamma^1_{10}\Gamma^0_{11} + \Gamma^1_{11}\Gamma^2_{12} + \Gamma^1_{11}\Gamma^3_{13} \quad (\text{A.9})$$

$$R_{rr} = \partial_t \frac{a\dot{a}}{c^2 a_p^2 \left(1 - \frac{r^2}{r_p^2}\right)} - 2\partial_r \frac{1}{r} + \frac{a\dot{a}}{c^2 a_p^2 \left(1 - \frac{r^2}{r_p^2}\right)} \frac{\dot{a}}{a} + 2\frac{r}{r_p^2 \left(1 - \frac{r^2}{r_p^2}\right)} \frac{1}{r} - 2\frac{1}{r^2} \quad (\text{A.10})$$

$$R_{rr} = \frac{a\ddot{a}}{c^2 a_p^2 \left(1 - \frac{r^2}{r_p^2}\right)} + \frac{\dot{a}^2}{c^2 a_p^2 \left(1 - \frac{r^2}{r_p^2}\right)} + \frac{\dot{a}^2}{c^2 a_p^2 \left(1 - \frac{r^2}{r_p^2}\right)} + \frac{2}{r_p^2 \left(1 - \frac{r^2}{r_p^2}\right)} \quad (\text{A.11})$$

$$R_{rr} = \frac{\left(\frac{a\ddot{a}}{a_p^2} + \frac{2\dot{a}^2}{a_p^2} + \frac{2c^2}{r_p^2}\right)}{c^2 \left(1 - \frac{r^2}{r_p^2}\right)} \quad (\text{A.12})$$

The $\theta - \theta$ component is

$$R_{\theta\theta} = R_{22} = \partial_0 \Gamma^0_{22} + \partial_1 \Gamma^1_{22} - \partial_2 \Gamma^3_{23} + \Gamma^0_{22} \Gamma^1_{01} + \Gamma^0_{22} \Gamma^3_{03} + \Gamma^1_{22} \Gamma^1_{11} + \Gamma^1_{22} \Gamma^3_{13} - \Gamma^2_{20} \Gamma^0_{22} - \Gamma^2_{21} \Gamma^1_{22} - \Gamma^3_{23} \Gamma^3_{32} \quad (\text{A.13})$$

$$R_{\theta\theta} = \partial_t \frac{r^2 a \ddot{a}}{c^2 a_p^2} - \partial_r r \left(1 - \frac{r^2}{r_p^2}\right) - \partial_\theta \cot(\theta) + \frac{r^2 a \dot{a}}{c^2 a_p^2} \frac{\dot{a}}{a} - r \left(1 - \frac{r^2}{r_p^2}\right) \frac{1}{r} - \cot^2(\theta) \quad (\text{A.14})$$

$$R_{\theta\theta} = \frac{r^2 a \ddot{a}}{c^2 a_p^2} + \frac{r^2 \dot{a}^2}{c^2 a_p^2} + \left(3 \frac{r^2}{r_p^2} - 1\right) + \csc^2(\theta) + \frac{r^2 \dot{a}^2}{c^2 a_p^2} - \left(1 - \frac{r^2}{r_p^2}\right) - \cot^2(\theta) \quad (\text{A.15})$$

$$R_{\theta\theta} = \frac{r^2 a \ddot{a}}{c^2 a_p^2} + 2 \frac{r^2 \dot{a}^2}{c^2 a_p^2} + \left(2 \frac{r^2}{r_p^2}\right) - 1 + \csc^2(\theta) - \cot^2(\theta) \quad (\text{A.16})$$

$$R_{\theta\theta} = \frac{r^2}{c^2} \left(\frac{a \ddot{a}}{a_p^2} + \frac{2 \dot{a}^2}{a_p^2} + \frac{2 c^2}{r_p^2} \right) \quad (\text{A.17})$$

The $\phi - \phi$ component is

$$R_{\phi\phi} = R_{33} = \partial_0 \Gamma^0_{33} + \partial_1 \Gamma^1_{33} + \partial_2 \Gamma^2_{33} + \Gamma^0_{33} \Gamma^1_{01} + \Gamma^0_{33} \Gamma^2_{02} + \Gamma^1_{33} \Gamma^1_{11} + \Gamma^1_{33} \Gamma^2_{12} - \Gamma^3_{30} \Gamma^0_{33} - \Gamma^3_{31} \Gamma^1_{33} - \Gamma^3_{32} \Gamma^2_{33} \quad (\text{A.18})$$

$$R_{\phi\phi} = R_{33} = \partial_t \frac{r^2 a \dot{a} \sin^2 \theta}{c^2 a_p^2} - \partial_r r \sin^2 \theta \left(1 - \frac{r^2}{r_p^2}\right) - \partial_\theta \sin \theta \cos \theta + 2 \frac{r^2 a \dot{a} \sin^2 \theta}{c^2 a_p^2} \frac{\dot{a}}{a} - r \sin^2 \theta \left(1 - \frac{r^2}{r_p^2}\right) \frac{r}{r_p^2 \left(1 - \frac{r^2}{r_p^2}\right)} \quad (\text{A.19})$$

$$- r \sin^2 \theta \left(1 - \frac{r^2}{r_p^2}\right) \frac{1}{r} - \frac{\dot{a} r^2 a \dot{a} \sin^2 \theta}{c^2 a_p^2} + r \sin^2 \theta \left(1 - \frac{r^2}{r_p^2}\right) \frac{1}{r} + \sin \theta \cos \theta \cot \theta$$

$$R_{\phi\phi} = R_{33} = \frac{r^2 a \ddot{a} \sin^2 \theta}{c^2 a_p^2} + \frac{r^2 \dot{a}^2 \sin^2 \theta}{c^2 a_p^2} - \sin^2 \theta \left(1 + 3 \frac{r^2}{r_p^2}\right) + \sin^2 \theta - \cos^2 \theta$$

$$+ \frac{r^2 \dot{a}^2 \sin^2 \theta}{c^2 a_p^2} - \sin^2 \theta \left(\frac{r^2}{r_p^2}\right) + \cos^2 \theta$$

$$R_{\phi\phi} = R_{33} = \frac{r^2 a \ddot{a} \sin^2 \theta}{c^2 a_p^2} + 2 \frac{r^2 \dot{a}^2 \sin^2 \theta}{c^2 a_p^2} + 2 \sin^2 \theta \frac{r^2}{r_p^2}$$

$$R_{\phi\phi} = \frac{r^2 \sin^2 \theta}{c^2} \left(\frac{a \ddot{a}}{a_p^2} + \frac{2 \dot{a}^2}{a_p^2} + \frac{2 c^2}{r_p^2} \right) \quad (\text{A.22})$$

The inverse metric tensor g^{uv} is

$$g^{uv} = \begin{pmatrix} \frac{1}{c^2} & 0 & 0 & 0 \\ 0 & -\left(1 - \frac{r^2}{r_p^2}\right) \frac{1}{\left(\frac{a^2}{a_p^2}\right)} & 0 & 0 \\ 0 & 0 & \frac{-1}{\left(\frac{a^2}{a_p^2}\right) r^2} & 0 \\ 0 & 0 & 0 & \frac{-1}{\left(\frac{a^2}{a_p^2}\right) r^2 \sin^2 \theta} \end{pmatrix} \quad (\text{A.23})$$

Finally, the Ricci scalar curvature $R = R_{uv} g^{uv}$ which equals the Ricci curvature tensor time the inverse metric tensor is

$$R = R_{uv} g^{uv} = \frac{-6}{c^2} \left(\frac{\ddot{a}}{a} + \frac{\dot{a}^2}{a^2} + \frac{c^2 a_p^2}{a^2 r_p^2} \right) \quad (\text{A.24})$$

References

- [1] Tolman R C 1931 On the theoretical requirements for a periodic behaviour of the universe *Phys. Rev.* **38** 1758–71
- [2] Minas G, Saridakis E N, Stavrinos P C and Triantafyllopoulos A 2019 Bounce cosmology in generalized modified gravities *Universe* **5** 74
- [3] Creswell J, Von Hausegger S, Jackson A D, Liu H and Naselsky P 2017 On the time lags of the LIGO signals *J. Cosmol. Astropart. Phys.* **2017** 013
- [4] Subramanian K 2015 The origin, evolution and signatures of primordial magnetic fields *Reports Prog. Phys.* **79**
- [5] Di Valentino E, Melchiorri A and Silk J 2020

- Planck evidence for a closed Universe and a possible crisis for cosmology *Nat. Astron.* **4** 196–203
- [6] Handley W 2021 Curvature tension: Evidence for a closed universe *Phys. Rev. D* **103** L041301
- [7] Meneghetti M, Davoli G, Bergamini P, Rosati P, Natarajan P, Giocoli C, Caminha G B, Metcalf R B, Rasia E, Borgani S, Calura F, Grillo C, Mercurio A and Vanzella E 2020 An excess of small-scale gravitational lenses observed in galaxy clusters *Science (80-.)*. **369** 1347–51
- [8] Umetsu K 2020 Cluster–galaxy weak lensing *Astron. Astrophys. Rev.* **28** 1–106
- [9] Riess A G 2020 The expansion of the Universe is faster than expected *Nat. Rev. Phys.* **2** 10–2
- [10] Ryskin G 2020 Vanishing vacuum energy *Astropart. Phys.* **115** 102387
- [11] Chae K H, Lelli F, Desmond H, McGaugh S S, Li P and Schombert J M 2020 Testing the strong equivalence principle: Detection of the external field effect in rotationally supported galaxies *arXiv* **904** 51
- [12] Ahmadi M, Alves B X R, Baker C J, Bertsche W, Capra A, Carruth C, Cesar C L, Charlton M, Cohen S, Collister R, Eriksson S, Evans A, Evetts N, Fajans J, Friesen T, Fujiwara M C, Gill D R, Granum P, Hangst J S, Hardy W N, Hayden M E, Hunter E D, Isaac C A, Johnson M A, Jones J M, Jones S A, Jonsell S, Khramov A, Knapp P, Kurchaninov L, Madsen N, Maxwell D, McKenna J T K, Menary S, Michan J M, Momose T, Munich J J, Olchanski K, Olin A, Pusa P, Rasmussen C, Robicheaux F, Sacramento R L, Sameed M, Sarid E, Silveira D M, So C, Starko D M, Stutter G, Tharp T D, Thompson R I, van der Werf D P and Wurtele J S 2020 Investigation of the fine structure of antihydrogen *Nature* **578** 375–80
- [13] Efstathiou G 2003 *Is the low cosmic microwave background quadrupole a signature of spatial curvature?* vol 343
- [14] Al-Fadhli M 2020 A new vision of the geometry of the cosmos as a twin-half closed Universe: accelerated expansion due to free fall gravitational attraction *NATASTRON-20012929 Lines 18-21 Submitt. 1400 GMT, 13/1/2020*
- [15] Minami Y and Komatsu E 2020 New Extraction of the Cosmic Birefringence from the Planck 2018 Polarization Data *Phys. Rev. Lett.* **125** 221301
- [16] Dirac P A M 1938 A new basis for cosmology *Proc. R. Soc. A Math. Phys. Eng. Sci.* **165** 199–208
- [17] Wilczynska M R, Webb J K, Bainbridge M, Barrow J D, Bosman S E I, Carswell R F, Dąbrowski M P, Dumont V, Lee C C, Leite A C, Leszczyńska K, Liske J, Marosek K, Martins C J A P, Milaković D, Molaro P and Pasquini L 2020 Four direct measurements of the fine-structure constant 13 billion years ago *Sci. Adv.* **6** eaay9672
- [18] Donoghue J F 2003 Spatial and temporal gradients in the cosmological constant *J. High Energy Phys.* **7** 1115–29
- [19] Uzan J P 2011 Varying constants, gravitation and cosmology *Living Rev. Relativ.* **14** 1–155
- [20] Landau L D 1986 *Theory of Elasticity* (Elsevier)
- [21] Rugh S E and Zinkernagel H 2000 The Quantum Vacuum and the Cosmological Constant Problem *Stud. Hist. Philos. Sci. Part B - Stud. Hist. Philos. Mod. Phys.* **33** 663–705
- [22] Wittenburg N, Kroupa P and Famaey B 2020 The formation of exponential disk galaxies in MOND *Astrophys. J.* **890** 173
- [23] S. M. Carroll 2003 *Spacetime and Geometry: An Introduction to General Relativity*
- [24] Dyer E and Hinterbichler K 2009 Boundary terms, variational principles, and higher derivative modified gravity *Phys. Rev. D - Part. Fields, Gravit. Cosmol.* **79**
- [25] Straub W O 2006 *Simple Derivation of the Weyl Conformal Tensor*
- [26] Kozameh C, Newman E, gravitation K T-G relativity and and 1985 undefined 1985 Conformal Einstein spaces *Springer*
- [27] Penrose R 2005 *The Road to Reality: A Complete Guide to the Laws of the Universe*
- [28] Lachi Eze-Rey M and Luminet J-P 2003 COSMIC TOPOLOGY *arXivgr-qc/9605010v2* 9 Jan 2003
- [29] Ellis G F R and van Elst H 1998 Cosmological

- models (Cargèse lectures 1998)
- [30] Straumann N 2013 General Relativity (Graduate Texts in Physics) *Springer* (Springer)
- [31] Ryden B 2006 *Introduction to Cosmology* (San Francisco, CA, USA: Addison Wesley, ISBN 0-8053-8912-1.)
- [32] Pavel Grinfeld 2013 *Introduction to Tensor Analysis and the Calculus of Moving Surfaces* (Springer)
- [33] Chen G C F, Fassnacht C D, Suyu S H, Rusu C E, Chan J H H, Wong K C, Auger M W, Hilbert S, Bonvin V, Birrer S, Millon M, Koopmans L V E, Lagattuta D J, McKean J P, Vegetti S, Courbin F, Ding X, Halkola A, Jee I, Shajib A J, Sluse D, Sonnenfeld A and Treu T 2019 A SHARP view of H0LiCOW: H₀ from three time-delay gravitational lens systems with adaptive optics imaging *Mon. Not. R. Astron. Soc.* **490** 1743–73
- [34] Copi C J, O’Dwyer M and Starkman G D 2016 The ISW effect and the lack of large-angle CMB temperature correlations *Mon. Not. R. Astron. Soc.* **463** 3305–10
- [35] Aguado D S, et al 2018 The fifteenth data release of the sloan digital sky surveys: First release of manga derives quantities, data visualization tools and stellar library *arXiv* **55** 23
- [36] Kashlinsky A, Atrio-Barandela F and Ebeling H 2011 Measuring the dark flow with public X-ray cluster data *Astrophys. J.* **732** 1–7
- [37] Hoffman Y, Pomarède D, Tully R B and Courtois H M 2017 The dipole repeller *Nat. Astron.* **1** 1–5
- [38] Chiang Y-K, Makiya R, Ménard B and Komatsu E 2020 The Cosmic Thermal History Probed by Sunyaev-Zeldovich Effect Tomography *arXiv*
- [39] Mannheim P D and Kazanas D 1989 Exact vacuum solution to conformal Weyl gravity and galactic rotation curves *Astrophys. J.* **342** 635
- [40] Sofue Y and Rubin V 2000 Rotation Curves of Spiral Galaxies *Annu. Rev. Astron. Astrophys.* **39** 137–74
- [41] Maeder A 2017 An alternative to the LCDM model: the case of scale invariance *Astrophys. J.* **834** 194
- [42] Brouwer M M, Visser M R, Dvornik A, Hoekstra H, Kuijken K, Valentijn E A, Bilicki M, Blake C, Brough S, Buddelmeijer H, Erben T, Heymans C, Hildebrandt H, Holwerda B W, Hopkins A M, Klaes D, Liske J, Loveday J, McFarland J, Nakajima R, Sifón C and Taylor E N 2016 First test of Verlinde’s theory of Emergent Gravity using Weak Gravitational Lensing measurements *Mon. Not. R. Astron. Soc.* **466** 2547–59
- [43] Chadwick E A, Hodgkinson T F and McDonald G S 2013 Gravitational theoretical development supporting MOND *Phys. Rev. D - Part. Fields, Gravit. Cosmol.* **88** 024036
- [44] Van Meter J R 2018 Dark-matter-like solutions to Einstein’s unified field equations *Phys. Rev. D* **97** 044018
- [45] Milgrom M 2019 MOND in galaxy groups: A superior sample *Phys. Rev. D* **99** 044041
- [46] Guo Q, Hu H, Zheng Z, Liao S, Du W, Mao S, Jiang L, Wang J, Peng Y, Gao L, Wang J and Wu H 2019 Further evidence for a population of dark-matter-deficient dwarf galaxies *Nat. Astron.* **4** 246–51
- [47] Sam Reid et al 2013 Fluid Pressure and Flow, PhET Interactive Simulations.